ACS APPLIED MATERIALS & INTERFACES

Research Article

Cite This: ACS Appl. Mater. Interfaces 2018, 10, 37651−37660

www.acsami.org

Polarity Control within One Monolayer at ZnO/GaN Heterointerface: (0001) Plane Inversion Domain Boundary

Siqian Li,*,† Huaping Lei,‡ Yi Wang,§ Md Barkat Ullah,∥ Jun Chen,† Vitaliy Avrutin,∥ Ümit Özgür,∥ Hadis Morkoç,∥ and Pierre Ruterana†

†CIMAP, UMR 6252 CNRS, ENSICAEN, UCBN, CEA, 6 Boulevard du Maréchal Juin, 14050 Caen Cedex, France

‡Key Laboratory of Materials Physics, Institute of Solid State Physics, Chinese Academy of Sciences, Hefei 230031, China

§Max Planck Institute for Solid State Research, Heisenbergstrasse 1, 70569 Stuttgart, Germany

∥Department of Electrical and Computer Engineering, Virginia Commonwealth University, Richmond, Virginia 23284, United States

Supporting Information

ABSTRACT: In semiconductor heterojunction, polarity critically governs the physical properties, with an impact on electronic or optoelectronic devices through the presence of pyroelectric and piezoelectric fields at the active heteropolar interface. In the present work, the abrupt O-polar ZnO/Ga-polar GaN heterointerface was successfully achieved by using high O/Zn ratio flux during the ZnO nucleation growth. Atomic-resolution high-angle annular dark-field and bright-field transmission electron microscopy observation revealed that this polarity inversion confines within one monolayer by forming the (0001) plane inversion domain boundary (IDB) at the ZnO/GaN heterointerface. Through theoretical calculation and topology analysis, the geometry of this IDB was determined to possess an octahedral Ga atomic layer in the interface, with one O/N layer symmetrically bonded at the tetrahedral site. The computed electronic structure of all considered IDBs revealed a metallic character at the heterointerface. More interestingly, the presence of two-dimensional (2D) hole gas (2DHG) or 2D electron gas (2DEG) is uncovered by investigating the chemical bonding and charge transfer at the heterointerface. This work not only clarifies the polarity control and interfacial configuration of the O-polar ZnO/Ga-polar GaN heterojunction but, more importantly, also gives insight into their further application on heterojunction field-effect transistors as well as hybrid ZnO/GaN optoelectronic devices. Moreover, such polarity control at the monolayer scale might have practical implications for heterojunction devices based on other polar semiconductors.

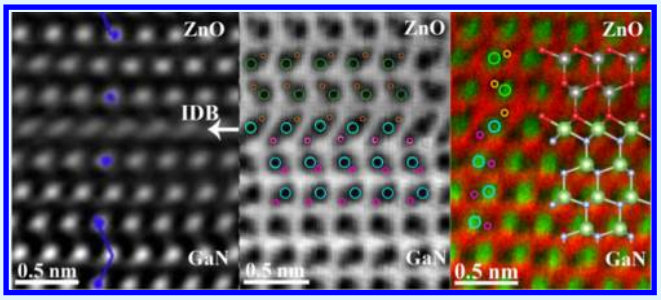

KEYWORDS: *ZnO/GaN heterointerface, (0001) plane IDBs, polarity control, energetic stability, 2DHG, 2DEG*

1. INTRODUCTION

The last two decades have shown intensive research on wurtzite semiconducting materials, primarily the group III nitrides and ZnO, for a wide range of potential applications, such as high-efficiency light emitters,[1] high-power, high-frequency transistors,[2,3] as well as spintronic devices.[4] Indeed, a whole industrial field was opened for solid-state lighting based on GaN, as soon as reliable p-type doping with Mg was established.[5] Of course, this is not yet the case in ZnO for which efficient p-doping is still a challenge, notwithstanding its large exciton bonding energy.[6]

Recently, ZnO-based heterojunction concept was introduced to operate two-dimensional electron gas (2DEG) with a sheer carrier density of 10^{13} cm^{-3} at the heterointerface without the need of doping,[7] which extends its application into heterojunction field-effect transistors (HFETs), such as ZnMgO/ZnO HFET, with electron mobility reported to reach as high as 10^6 cm^2 V^{-1} s^{-1} at low temperature.[8] However, limited availability and high price of native ZnO substrate necessitate establishing growth of high-quality ZnO structure on foreign substrates, for instance III nitrides,[9] Al_2O_3,[10,11] and SiC.[12] However, due to the large lattice mismatch, the epitaxial ZnO layers are always plagued with high densities of extended defects inherent to the wurtzite structure.[13−15] Detrimental effects of these defects on the performances of the related devices have been the subject of numerous reports.[16−20] For instance, the basal and prismatic stacking faults in ZnO were reported to exhibit low formation energies and tend to coexist with large densities of point defects.[13,14] For the prismatic $\{10\bar{1}0\}$ inversion domain boundary (IDB), which exhibits two stable atomic configurations,[21−24] this type of boundary was found to not induce electronic states in the band gap but could attract charged point defects and build up an electrical potential for the minority carriers in both p- and n-type

Received: July 19, 2018
Accepted: October 3, 2018
Published: October 3, 2018

DOI: 10.1021/acsami.8b12202
ACS Appl. Mater. Interfaces 2018, 10, 37651−37660

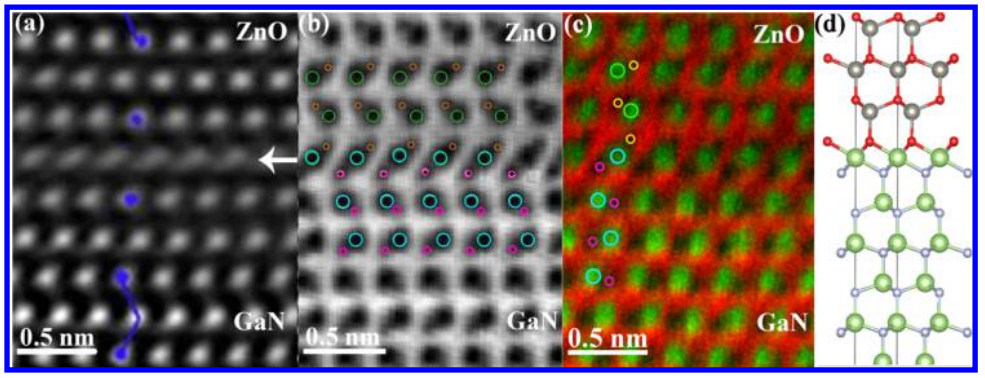

Figure 1. STEM images of O-polar ZnO/Ga-polar GaN heterointerface. (a) HAADF image of O-polar ZnO/Ga-polar GaN heterointerface. The white arrow shows the interface. The blue dots and lines underline the stacking sequences. (b) Simultaneous ABF image where atoms have been superimposed. Big circles indicate metal atoms and small circles denote nonmetal atoms. (c) Overlap of the HAADF and ABF images showing the interface configuration. (d) Corresponding atomic model of the (0001) plane IDB.

ZnOs.[15] Obviously, to fabricate high-performance devices, it is necessary to fabricate high-quality ZnO thin films. To further improve the structural perfection of ZnO films, (0001)-GaN/c-sapphire template is considered as one of the best substrates for epitaxial growth because the 1.8% of the lattice mismatch between GaN and ZnO is 10 times smaller than that with sapphire. This improvement in high-quality ZnO film growth would indeed open the way for optimization of devices performance.[25] The predicted electron velocity in bulk ZnO reaches 3.1×10^7 cm s^{-1},[26,27] exceeding that in GaN (2.9×10^7 cm s^{-1}).[28] When combined with inexpensive epitaxial technology, this feature makes ZnO an attractive choice for high-power, high-frequency FETs (note that p-type problem is not an obstacle for these unipolar devices relying on electron conduction). In particular, theory predicts superior performance of ZnO-based FETs in terahertz range as compared to GaAs.[27]

The realization of full potential of ZnO-based heterostructures on GaN in electronic devices requires an insight into the properties of the ZnO/GaN heterointerfaces at the atomic scale. At the interface, one not only faces purely crystallographic and chemical relationship but also requires a precise control on the polarity relationship. As an example, in a number of reports published on the luminescence properties of p-GaN/n-ZnO heterojunctions, the emission was observed either from the GaN[29,30] or the ZnO side.[31−33] However, as was reported by Schuster et al. for nearly defect-free/p-GaN/n-ZnO nanowires,[34] strong excitonic UV emission originating from the ZnO side of the interface as well as stimulated emission can be controllably attained from the ZnO side. Until now, attempts to attain control of the layer polarity at the ZnO/GaN heterostructure are scarce, mainly consisting of the insertion of ultrathin (4 nm) Ga_2O_3, which helped change the polarity of the overgrown ZnO to O-polar on top of a Ga-polar template.[34,35] However, for device application, an abrupt and clean interface between the two semiconductors is the most efficient way to achieve the best performance. In this vein, early attempt to grow Ga-polar GaN on O-polar ZnO by pulsed laser deposition reported that this could take place at room temperature, whereas it was necessary to use a low temperature buffer layer to achieve similar result at 700 °C.[36,37] Recently, by close tuning of the growth conditions in molecular beam epitaxy (MBE), complete reversal of polarity of a ZnO layer growing on a Ga-polar GaN template within one monolayer could be obtained.[38] But, the details of the atomic structures of this ZnO/GaN heterointerface and the corresponding physical properties have not been clarified yet. Clearly, this ZnO/GaN heterointerface is (0001) plane IDB and a number of reports on its investigation mainly focus on polycrystalline wurtzite BeO[39] and ZnO[40] using either optical or high-resolution transmission electron microscopy. In agreement with the geometrical models proposed by Kim and Goo,[40] the study of the surface energy points out to the eight atomic configurations of the (0001) IDB in wurtzite. However, until now, neither a systematic investigation of their structural, energetic, and electronic stability not a detailed experimental analysis of the stable atomic structure has been reported.

In this article, we report on a systematic investigation of a one monolayer transition from Ga-polar GaN to O-polar ZnO heterostructure using scanning transmission electron microscopy (STEM), particularly in the high-angle annular dark-field and annular bright-field mode (HAADF, ABF) to clarify the atomic structure and chemical composition. To gain insight into the genesis of the experimental observations, a detailed theoretical analysis based on density functional theory (DFT) is used to elucidate the chemical bonding character and electronic property of the heterointerfaces.

2. EXPERIMENTAL OBSERVATIONS

TEM investigation on polarity-inverted ZnO/GaN heterointerface is shown in Figure 1. The sample information and experimental condition are given in the Supporting Information (SI). As pointed out by white arrow (HAADF image of Figure 1a), only one monolayer in this ZnO/GaN heterointerface exhibits a change in contrast, which originates from the abrupt epitaxial growth that takes place in the (0001) GaN surface. Further, in GaN template and ZnO epilayer, a change in stacking sequence, as illustrated by blue dots and lines, reveals the occurrence of polarity inversion between two layers.[41] In the ABF image recorded simultaneously (Figure 1b), a clear atomic resolution is obtained and the light atom positions are now well visible. The characteristic polarity dumbbell pairs of wurtzite crystal are clearly resolved with the presence of the lighter contrast zigzag below or above the darker atomic positions (Ga, Zn). The interface plane comes out as only one monolayer that exhibits a different geometry with respect to the perfect wurtzite structure. Otherwise, on each side of the interface, the hexagonal "-ABAB-" stacking is clearly reserved and the polarity can be identified as O-polar in ZnO and Ga-polar in GaN. Figure 1c is the superimposition of HAADF and ABF images in which the large green spots correspond to the intensities where the metal atoms are dominant. Now, the abrupt ZnO/GaN heterointerface is evidently identified as a contribution of the metal layer. And the whole stacking sequence of

DOI: 10.1021/acsami.8b12202
ACS Appl. Mater. Interfaces 2018, 10, 37651−37660

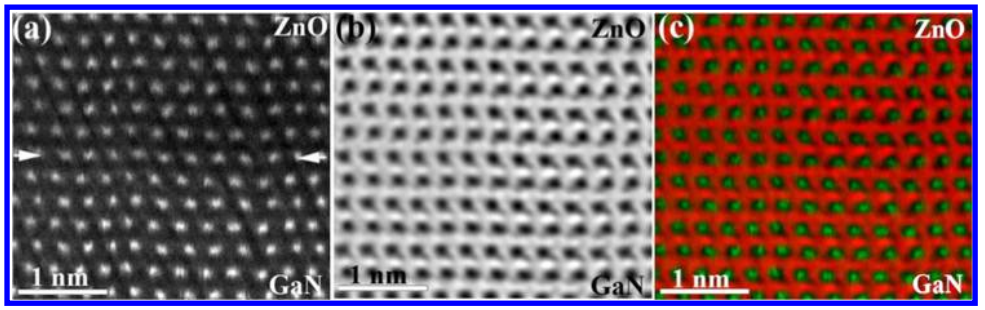

Figure 2. STEM images of Zn-polar ZnO/Ga-polar GaN heterointerface. (a) HAADF image where the interface position is pointed out by white arrows. (b) ABF image recorded on the same area as in (a). (c) A superposition of the HAADF and ABF images showing the continuous polarity.

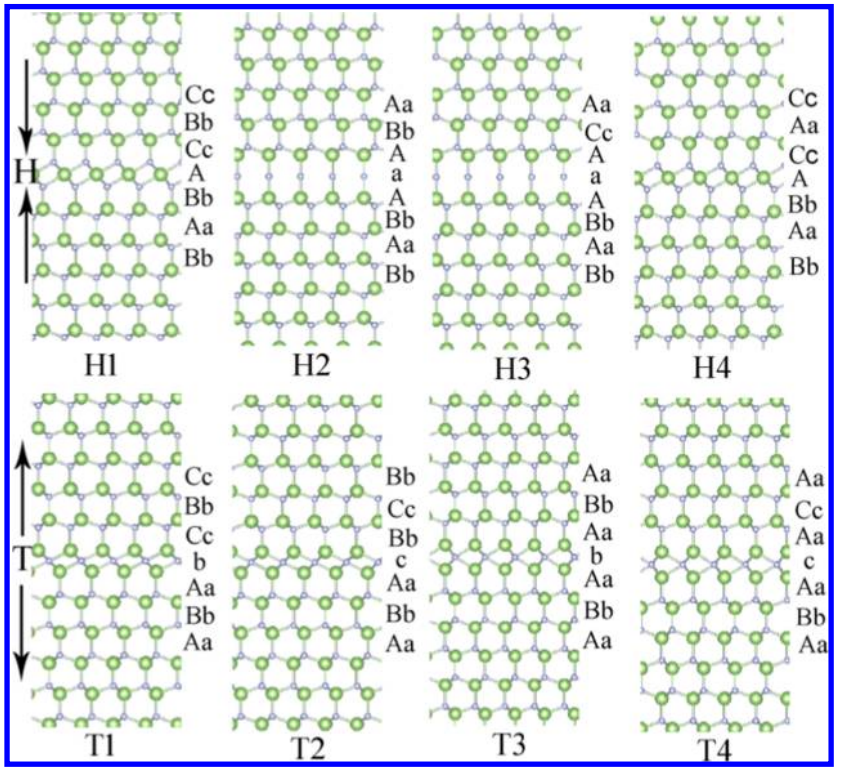

Figure 3. Geometric models of the eight (0001) plane IDBs projected along the [11$\bar{2}$0] direction. The green and blue balls represent the metal and nonmetal atoms, respectively. The arrows indicate the polarity from metal atoms to nonmetal atoms. The wurtzite stacking is shown for each model.

the heterostructure can be directly deduced to AaBbA-cCaAc (H4 IDB) by following the same definition as in ref 40. The corresponding atomic model is shown in Figure 1d.

When the polarity inversion was not initiated by tuning the right O/Zn ratio, the polarity of the substrate extends to the ZnO epilayer and the interface geometry is completely reserved. As seen in the HAADF image of Figure 2a, only a faint change in chemical contrast permits delineation of the ZnO/GaN interface (see white arrows). The corresponding ABF image (Figure 2b) displays a perfect transfer of the cation−anion sequence through the interface. This polarity continuity also can be underlined directly in the superimposition of the HAADF and ABF images (Figure 2c) in which a Zn-polar ZnO/Ga-polar GaN heterostructure is shown.

Although the TEM observations clearly displayed the geometry of ZnO/GaN heterointerface and proved that the inversion operation has taken place at a metal atomic layer, the exact elemental composition of the interfacial monolayer (cation−anion) should be subjected to a more intimate examination. Previously, Kim and Goo[40] proposed eight possible (0001) plane IDBs in ZnO without taking into account the nonstoichiometric wrong bonds, which are considered energetically unfavorable depending on the topology analysis combined with the TEM measurement. One may assume that these theoretical configurations also agree with the studied ZnO/GaN heterointerface because the lattice mismatch between ZnO and GaN is moderate (1.8%). Considering the reduced surface mobility in the used MBE process at quite low temperature (300 °C),[38] we may suspect that mixtures of atomic species (Zn/Ga, O/N) at the interface should remain at the level of dopants and shall not be considered in modeling the dominant properties of the (0001) plane IDB at the heterointerface. Moreover, because the GaN surface was thermally precleaned at high temperature and the use of O/Zn ratio flux is as high as 6.0, one may conclude that the growth was initiated with a Ga-terminated surface leading to a −N−Ga−O−Zn− (type A) interface alignment. However, we could also consider the extreme case of a monolayer shift of the interface to the next layer to form a −Ga−N−Zn−O− (type B) interface. From the above points, for each IDB model, two types of interfaces (type A and type B) are considered in the following simulation sections. For convenience, simplified expression in the form of H(A) IDB is also used to represent an H IDB with type A interface in the following discussion, and so forth.

DOI: 10.1021/acsami.8b12202
ACS Appl. Mater. Interfaces 2018, 10, 37651−37660

3. METHODOLOGY

First-principle calculations are performed using the Vienna ab inito simulation package.[42,43] The exchange correlation functional adopts the generalized gradient approximation with the Perdew−Burke−Ernzerhof scheme. The interaction between core and valence electrons is described by the projector-augmented-wave pseudopotential.[44] A 21 × 21 × 1 Monkhorst−Pack γ mesh is applied for Brillouin zone sampling; the tolerance of energy and force convergence is set to 10^{-6} eV and 0.01 eV $Å^{-1}$, respectively.

The geometrical models of the eight possible (0001) plane IDBs proposed by Kim and Goo[40] are depicted in Figure 3. Following the original notation,[40] in H and T IDBs, the polarity is head-to-head and tail-to-tail, respectively; the wurtzite stacking sequence labeled along side is preserved through the whole structure. As can be seen, H1 and H4 IDBs exhibit similar structural features: a metal atomic layer located at the octahedral position sharing six nearest neighbor nonmetallic atoms at the interface, which, in turn, bond to the adjacent layer of the tetrahedrally positioned metal atoms. The difference between H1 and H4 IDB comes from the next-nearest neighbor atomic bilayer, which shifts from Bb location in H1 to Aa in H4. In H2 and H3 IDBs, an aligned metal−nonmetal−metal atomic arrangement is shown: the nonmetal atomic layer at the interface binds to two metal layers with an angle of 180° in deviation of tetrahedral occupation. Regarding T IDBs, the interfaces are made of a nonmetallic atomic layer where each atom is surrounded by six nearest neighboring metal atoms situated at tetrahedral locations.

Depending on the geometry reviewed above, the (0001) plane IDBs at the ZnO/GaN interface are constructed using slab models with consideration of two types of interfaces. Each supercell contains only one boundary at the interface, with nine bilayers on both sides along the [0001] direction. The detailed interface alignments can be seen in Figure 5 (type A interface) and Figure S1 (type B interface). The use of slab scheme implies a infinite planar defect on the (0001) plane. Pseudo-hydrogen atoms with fractional charge are used to saturate the terminated surface and a vacuum layer of 24.4 Å thickness is set to avoid the artificial interaction between the image slabs.[45] During the structural relaxation, the top two bilayers of GaN and the whole ZnO epilayer are relaxed, whereas the rest of the GaN atoms are fixed at their bulk positions to simulate the substrate.

4. RESULTS AND DISCUSSION

4.1. Structural Stability. The thermodynamic stability of the 16 IDBs is evaluated by computing their relative formation energies γ_{form}, and further formation energy approximation under local equilibrium chemical environment of growth processing is shown in the SI.

Figure 4 shows the relative formation energies of those IDBs under different processing condition. In the results, negative value of γ_{from} demonstrates the relatively lower formation energy compared with the reference. For all the IDBs considered, it is found that the four structure pairs H1/H4, H2/H3, T1/T2, and T3/T4 IDBs exhibit very similar energy variation, respectively, independent of the interface alignment. When comparing their corresponding stacking sequence, it is understandable that the structural deviation coming from the next-nearest neighbors has small influence on the thermodynamical stability of the IDBs.

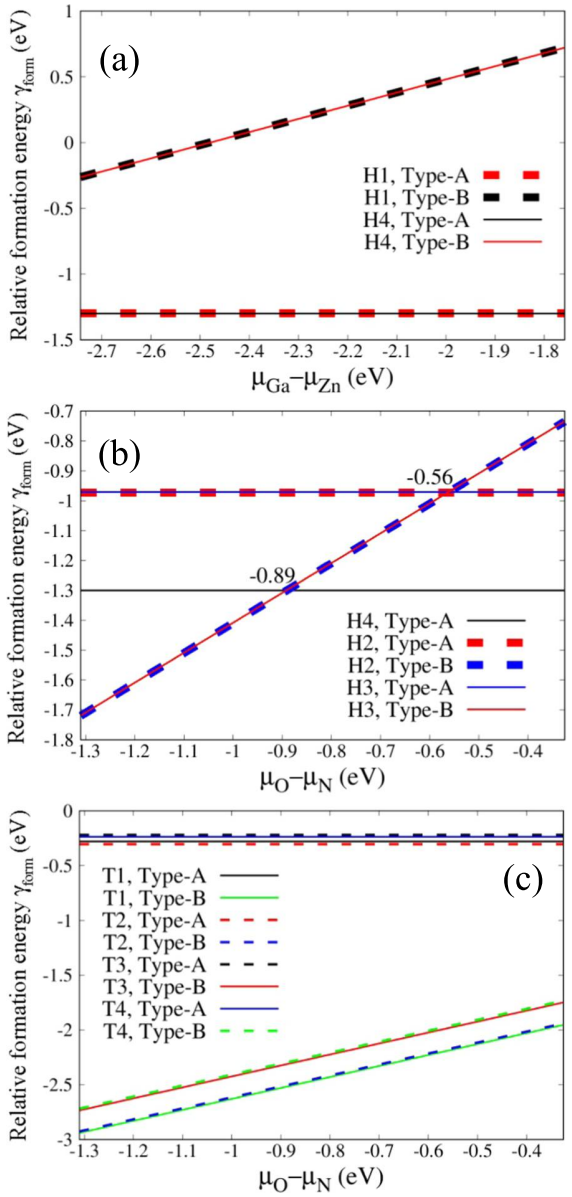

Figure 4. Relative formation energy of the (0001) plane IDBs at ZnO/GaN heterointerface with type A and type B interfaces: (a) H1/H4 IDBs, (b) H2/H3 IDBs in comparison to H4(A) IDB, and (c) T1−T4 IDBs.

In Figure 4a, independent of the $\mu_{Ga} - \mu_{Zn}$ variation, H1/H4(A) IDBs are more stable than H1/H4(B) IDBs, and the relative formation energy of H4(A) IDB is 2 meV lower than that of H1(A) IDB. It suggests that the H4(A) IDB is always more energetically favored than the other three IDBs. The relative formation energies of H2/H3(B) IDBs are smaller than those of H2/H3(A) IDBs when the $\mu_O - \mu_N$ value is lower than −0.56 eV, as shown in Figure 4b. When the $\mu_O - \mu_N$ value increases above −0.56 eV, H2/H3(A) IDBs become more stable. Taking H4(A) IDB as a reference (black line in Figure 4b), it is found that H2/H3(A) IDBs always have a higher formation energy, namely, lesser energetically favored than the H4(A) one. However, with the $\mu_O - \mu_N$ value below −0.89 eV, H2/H3(B) IDBs are the most stable configurations in all H IDBs. Once $\mu_O - \mu_N > -0.89$ eV, H4(A) IDB becomes the most stable configuration among all H IDBs.

DOI: 10.1021/acsami.8b12202
ACS Appl. Mater. Interfaces 2018, 10, 37651−37660

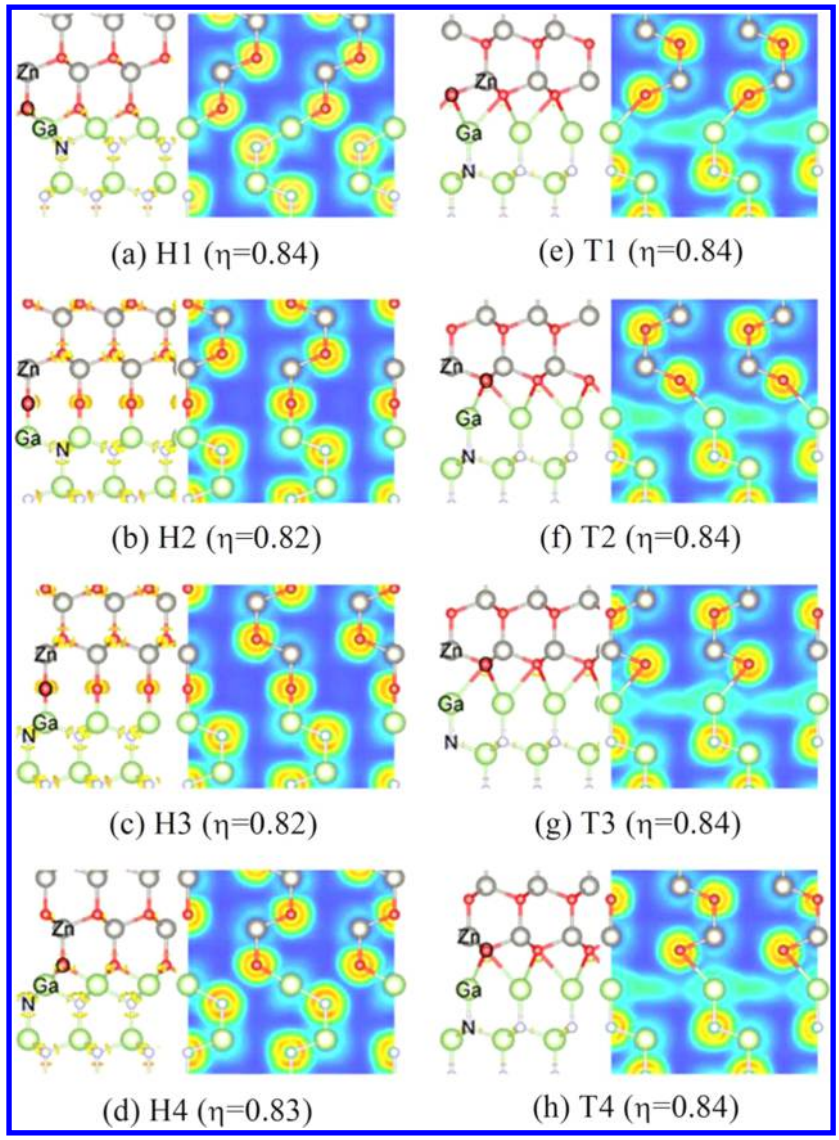

Figure 5. ELF of the (0001) plane IDBs in the ZnO/GaN heterointerface with type A interface: (a–d) H IDBs and (e–h) T IDBs. In each panel on the left side is ELF isosurface contour, whereas that on the right side is 2D contour slice of ELF crossing the $(11\bar{2}0)$ atomic plane. Interfacial atom alignment –Zn–O–Ga–N– is labeled by element symbols, and Zn, O, Ga, and N atoms are represented by gray, red, green, and silver balls, respectively.

In regard to T IDBs, because the polarity arrangement has changed, their thermodynamic stability should be individually discussed without the comparison to H counterparts. Figure 4c clearly shows that T1/T2(B) IDBs are more stable than the other T IDBs within the whole range of chemical potential difference $\mu_O - \mu_N$. Additionally, between these two IDBs, the formation energy of T1(B) IDB is 14 meV smaller than that of T2(B) IDB. It means that T1 IDB with type B interface is the most stable configuration with respect to all T IDBs in the ZnO/GaN heterointerface.

Considering the growth condition of high O/Zn ratio in the MBE process, the constraint of chemical potential difference $\mu_O - \mu_N$ is larger than −0.89 eV, indicating the most energetically stable H4(A) IDB is the best appropriate structure to describe the experimental results.

4.2. Chemical Bonding and Bader Population Analysis. After discussing the energetics of the (0001) plane IDBs, the chemical bonding and the charge transfer in the vicinity of the ZnO/GaN heterointerface are further investigated by means of electron localization function (ELF)[46−48] and Bader charge analysis.

Figures 5 and S1 illustrate the ELF isosurface contours for those IDBs projected along the $[11\bar{2}0]$ direction (left panels of Figures 5 and S1a–h). As seen in ZnO and GaN bulk regions, the electron localization domains of the Zn–O and Ga–N bonds localize more toward the O/N atoms due to their large electronegativity. By increasing the isosurface value, those electron localization domains spatially bifurcate into four irreducible domains (yellow regions in the left panels of Figures 5 and S1), named as bonding attractors, which correspond to the four bonds in a perfect structure. The corresponding 2D contour slices are displayed on the right panels of Figures 5 and S1a–h using a color scheme in which the colors range from blue through yellow to brown while ELF increases from 0 to 1. The O/N atom positions are seen as the large brown-yellow annular regions in right panels of Figure 5 and S1a–h. It indicates that the high localized electrons are found in the regions. The Zn/Ga atoms are associated with a

DOI: 10.1021/acsami.8b12202
ACS Appl. Mater. Interfaces 2018, 10, 37651−37660

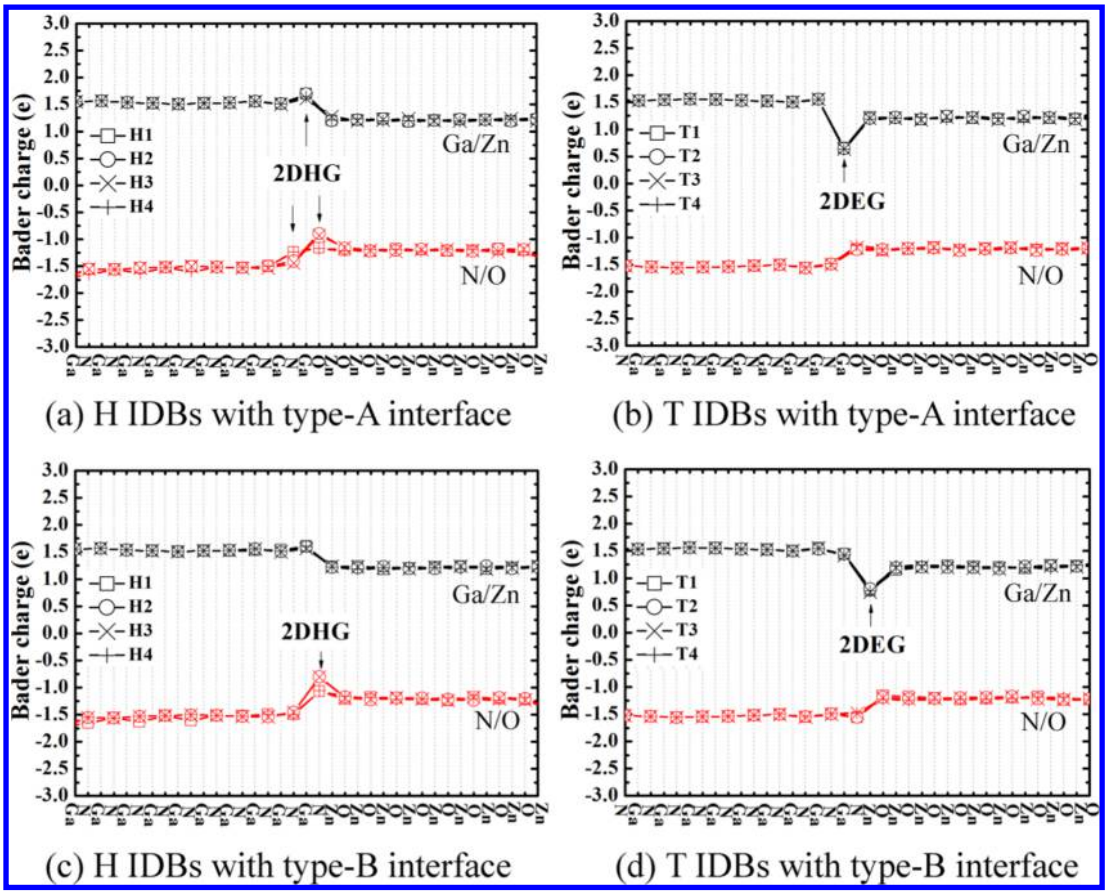

Figure 6. Bader population analysis of the (0001) plane IDBs in the ZnO/GaN heterointerface: (a) H(A) IDBs, (b) T(A) IDBs, (c) H(B) IDBs, and (d) T(B) IDBs.

small ELF value with a light blue ring. The polarized covalent character of the Zn−O and the Ga−N bonds can be seen in the oval shaped localization domains of the O/N atoms pointing toward the Zn/Ga domains.

In regard to H1/H4(A) IDBs, electron localization domains resolve into four bonding attractors around the interfacial O/N atoms, which are consistent with those in the bulk regions, as shown in the left panels of Figure 5a,d. However, in H1/H4(B) IDBs (see the left panels of Figure S1a,d), the localization attractor along the N−Zn bonds appears to be a large domain located above the N atom, a deviation from tetrahedral the configuration, which may respond to the high energy shown in Figure 4a. As for H2/H3(A) IDBs, the electron localization domain exhibits a spherical section around the interface O atom, as shown in the left panels of Figure 5b,c. However, in Figure S1b,c, interfacial N atom in H2/H3(B) IDBs has two bonding attractors located at an angle of 180° at the links of Zn−N and N−Ga. The 2D contour slices exhibit no obvious change in H IDBs relative to the perfect crystal as described in their corresponding right panels of Figures 5a−d and S1a−d.

The electron localization domains of either Zn−O−Ga or Zn−N−Ga chains in T IDBs are located close to the intermediate O/N atoms and exhibit more dispersion because the O/N atoms are located at the octahedral site, which corresponds to more nearest-neighbor atoms, as shown in the left panels of Figures 5e−h and S1e−h. Additionally, more interesting is that all the 2D contour slices exhibit a visible electron delocalization with the ELF value of about 0.5 at the interfacial Ga/Zn atom layer in T(A/B) IDBs, indicating the formation of a homogeneous electron gas at the boundaries,[47] as shown in the right panels of Figures 5e−h and S1e−h.

Bader charge analysis on individual atom layer is implemented along the [0001] direction to quantify the charge transfer in IDBs. As shown in Figure 6a for all H(A) IDBs, the interfacial Ga atom has a charge of +1.7 e^-, 0.2 e^- more than the value in a perfect crystal (+1.5 e^-). This indicates a positively charged interfacial Ga layer in H(A) IDBs. Additionally, the adjacent N or O layer in H1/H4 or H2/H3 IDBs is also found to accept an extra charge of +0.3 e^- per atom in comparison to those in the bulk regions, respectively. In the same vein, Bader charge shown in Figure 6c exhibits a positively charged N layer at H(B) IDBs with an additional charge of around +0.7 e^- gained by each N atom. This hole concentration at one (or even two) atom layer points to the existence of two-dimensional hole gas (2DHG) in H IDBs. However, because the ELF does not visualize the hole density, there is no variation uncovered in 2D contour slices of ELF (right panels of Figures 5 and S1a−d). Regarding the T IDBs, the interfacial Ga or Zn atoms accept an extra charge of −1.0 e^- each in the type A interface and −0.5 e^- each in the type B interface relative to those in the bulk region. And this electron accumulation in the interfacial monolayer does not extend vertically to the adjacent atom layers, strongly suggesting the occurrence of 2DEG and perfectly agrees with the ELF results shown in Figures 5 and S1e−h. The present DFT calculations constitute a quantum mechanical explanation of the results that were recently reported based on the effective

DOI: 10.1021/acsami.8b12202
ACS Appl. Mater. Interfaces 2018, 10, 37651−37660

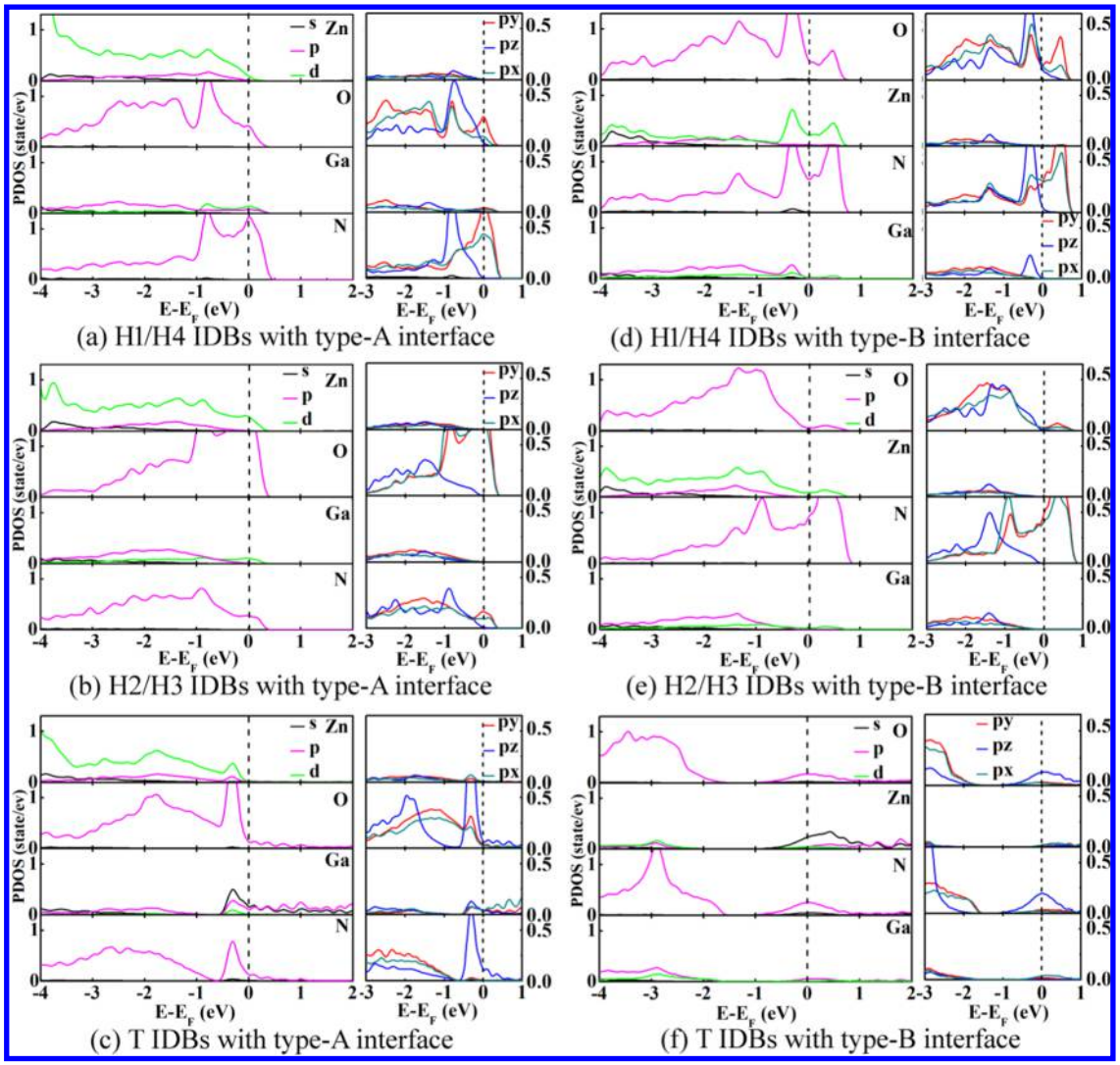

Figure 7. PDOS of the individual interface atom layer in each IDB with type A interface (a−c), and type B interface (d−f). The atom sequence follows the interface atomic chain labeled in Figures 5 and S1. Fermi level is highlighted by dashed line at zero position.

mass approach, where the formation of interface charges was reported to originate from the synergetic effect of piezoelectric and spontaneous polarization in such heterostructures.[34]

4.3. Electronic Structure of IDBs. The computed partial density of states (PDOS) on individual atom layer at each IDB are plotted in Figure 7, in which H1/H4, H2/H3, and all T IDBs exhibit similar profiles within type A and type B interface, respectively. Moreover, the corresponding PDOS onto the p (p_x, p_y, and p_z) orbitals of the atoms near the valance band edge are provided to further illustrate the electron contribution (see right panel of each figure).

As can be seen in Figure 7a,b,d,e, all H IDBs are observed to be metallic, as there is nonzero DOS across the Fermi level position. The metallic behavior of H(A) IDBs mainly comes from the contribution of Ga/Zn 3d, 4p and N/O 2p orbitals around the Fermi level position. The hybridization peak emerging across the Fermi level came from the strong interaction of Ga/Zn 3d and N/O 2p orbitals, confirming the metallic character of H(B) IDBs (Figure 7d,e). Combining with the ELF and Bader charge analysis above, the empty states just above the Fermi level may serve as p-type interface states in H IDBs. The split PDOS onto p_x, p_y, and p_z orbitals of the interfacial atoms reveal that contributions of N/O p orbitals on the valence band edge are strongly dependent on the local topology of the IDBs. As shown for H1/H4 IDBs in Figures 5 and S1a,d, the interfacial cations are located at the octahedral site and bounded with symmetric O/N atoms in the tetrahedral position. The number of cation−anion bonds and their bond angles are deviated from the perfect crystal. Therefore, the hybridization states at band edge are intensive in density, with the contribution mainly coming from N/O p_x, p_y, and p_z orbitals below 0 eV, whereas the hybridization states above the Fermi level originate from N/O p_x and p_y orbitals. In H2/H3 IDBs that have linear atomic chain in the *z*-direction, with the cations located at the tetrahedral site (seen in Figures 5 and S1b,c), the p_z orbitals of the interfacial O atom in Figure 7b and N atom in Figure 7e stay identical as those in perfect wurtzite structure, whereas the p_y and p_z orbitals are strongly hybridized with Zn/Ga 4d orbitals at the valence band edge. As for the rest band immediately below the valence band maximum, states of Zn/Ga 3d, 4p and N/O 2p orbitals are dominant. The high density of Zn 3d orbital in the entire valence band range and the strong coupling interaction of p−d orbitals at the valence band maximum fully agree with the experimental results from the X-ray photoelectron spectrosco-

DOI: 10.1021/acsami.8b12202
ACS Appl. Mater. Interfaces 2018, 10, 37651−37660

py[49] and the theoretical investigations obtained by all-electron band structure calculation[50] and LDA + U method.[51]

PDOS of T(A) IDBs exhibit the same electron contribution of Zn/Ga 3d, 4p and N/O 2p orbitals as the IDBs discussed above in the middle of the valence band (energy range from −4 to −1 eV), but with bands extended in energy. The localized states that appear at around −0.3 eV are mainly contributed from Zn 3d, 4p, O/N 2p (p_x, p_y, p_z), as well as Ga 4s, 4p, and 3d orbitals. This states extend across the Fermi level with all the Ga orbitals remarkably intensive, corresponding to the already pointed out negatively charged Ga atomic layer in the ELF and Bader charge analysis. Similarly, all the Zn orbitals at T(B) IDBs are remarkably intense and strongly hybridize with O/N 3p and Ga 4p orbitals around the Fermi level, supporting the electron accumulation at the interfacial Zn layer as discussed above. The bands in the low-energy range shift below and extend in energy with the same electron orbital contribution as in other IDBs.

Through detailed experimental observations, we have specifically addressed an H IDB at O-polar ZnO/Ga-polar GaN heterointerface and this polarity reversal took place in one metal monolayer all over the sample surface. The H4(A) model is clearly shown to be the most stable with the −Zn−O−Ga−N− interface alignment, where the interface layer is formed by Ga atoms. This is in complete agreement with the growth conditions, where the O/Zn ratio was high[38] and the surface mobility is quite lower in the P-MBE process. As unveiled above, the H IDBs exhibit a 2DHG, whereas the T ones present a 2DEG at the interfaces. Indeed, as free standing GaN substrate is available, this investigation finds direct application when the growth of ZnO with polarity reversal within one monolayer will be made on the (0001) surface for the specific device and opens new avenues in novel electronic and optoelectronic devices through a selective area surface modification.

5. CONCLUSIONS

In summary, O-polar ZnO/Ga-polar GaN heterostructure has been achieved using a high O/Zn ratio, above the critical value of 1.5, during the low-temperature P-MBE growth process. Detailed high-resolution HAADF and ABF STEM investigations unveiled that the polarity inversion took place within one monolayer, in which the metal atoms are dominant, to form the (0001) plane IDB at the ZnO/GaN heterointerfaces. Systematical theory simulation of H and T type polarity alignment at the ZnO/GaN heterointerface has been performed with the consideration of −Zn−O−Ga−N− and −O−Zn−N−Ga− interfaces. In contrast with the earlier work carried out on polycrystalline ZnO that predicted a H3 IDB, H4 IDB with a −Zn−O−Ga−N− type interface at the O-polar ZnO/Ga-polar GaN heterointerface matches the experimental topology very well and comes to be more energetically stable by comparing the relative formation energy. In a detailed analysis of the chemical bonding and charge transfer at those IDBs, it is shown that, independent of atomic sequences, the H IDBs exhibit a 2DHG with one or two interfacial atom layers positively charged. However, the T IDBs display a visible electron delocalization with an ELF value of around 0.5 at the interfacial Ga/Zn layers, and the layers gained extra 1.0/0.5 e^- electron per atom, suggesting the formation of 2DEG. The PDOS analysis uncovered a metallic nature at the 16 IDBs, as there are nonzero electron states crossing the Fermi level, which are mainly originated from Zn/Ga 3d (H IDBs), 4s (T IDBs) and O/N 2p orbitals. In this instance, we have unveiled a general property of such interfaces in agreement with a recent report based on the analysis of the transport properties in interplay with the polar character of these materials. Of course, this insight into the physico-chemistry of the ZnO/GaN interface at the monolayer scale might provide means for controlling polarity in heterojunction devices based on other polar material systems, including III nitrides and II−VI semiconductors. The desirable property suggests that the fabricated O-polar ZnO/Ga-polar GaN heterostructure could be a promising material for high electron mobility transistors for high-frequency and high-power applications in telecommunication.

■ ASSOCIATED CONTENT

Supporting Information

The Supporting Information is available free of charge on the ACS Publications website at DOI: 10.1021/acsami.8b12202.

Description of ZnO/GaN heterostructure growth and STEM (HAADF and ABF techniques) measurement conditions (Section 1); detailed derivation process of relative formation energy (Section 2); ELF results of (0001) plane IDBs in ZnO/GaN heterointerface with type B interface (Figure S1) (PDF)

■ AUTHOR INFORMATION

Corresponding Author

*E-mail: siqian.li@ensicaen.fr.

ORCID

Siqian Li: 0000-0003-3348-1587

Notes

The authors declare no competing financial interest.

■ ACKNOWLEDGMENTS

The calculations have been carried through the computer resources of CRIANN "Centre Régional Informatique et d'Applications Numériques de Normandie" under project No. 2016009, which is gratefully acknowledged. S. Q. Li is grateful to the China Scholarship Council for financial support under the file number 201508420147. H. P. Lei acknowledges the National Science Foundation of China under Grant No. 11575230 (NSFC) and the Young Foundation of the director of Institute of Solid State Physics, Chinese Academy of Sciences under Grant No. 2016DFY23 for their financial support. At Virginia Commonwealth University, this work was supported by Air Force Office of Scientific Research (AFOSR) under Grant No. FA9550-12-1-0094.

■ REFERENCES

(1) Guo, X. L.; Choi, J. H.; Tabata, H.; Kawai, T. Fabrication and Optoelectronic Properties of a Transparent ZnO Homostructural Light-Emitting Diode. *Jpn. J. Appl. Phys.* **2001**, *40*, L177−L180.

(2) Mitra, A.; Thareja, R. K.; Ganesanc, V.; Guptac, A.; Sahooa, P. K.; Kulkarni, V. N. Synthesis and Characterization of ZnO Thin Films for UV Laser. *Appl. Surf. Sci.* **2001**, *174*, 232−239.

(3) Hoffman, R. L.; Norris, B. J.; Wager, J. F. ZnO-based Transparent Thin-Film Transistors. *Appl. Phys. Lett.* **2003**, *82*, 733−735.

(4) Ohta, H.; Mizoguchi, H.; Hirano, M.; Narushima, M.; Kamiya, H. T.; Hosono, H. Fabrication and Characterization of Heteroepitaxial p-n Junction Diode Composed of Wide-gap Oxide Semiconductors p-$ZnRh_2O_4$/n-ZnO. *Appl. Phys. Lett.* **2003**, *82*, 823−825.

DOI: 10.1021/acsami.8b12202
ACS Appl. Mater. Interfaces 2018, 10, 37651−37660

(5) Amano, H.; Kito, M.; Hiramatsu, K.; Akasaki, I. P-Type Conduction in Mg-Doped GaN Treated with Low-Energy Electron Beam Irradiation (LEEBI). *Jpn. J. Appl. Phys.* **1989**, *28*, L2112−L21148.
(6) Özgür, Ü.; Alivov, Y. I.; Liu, C.; Teke, A.; Reshchikov, M. A.; Dogan, S.; Avrutin, V.; Cho, S. J.; Morkoç, H. A Comprehensive Review of ZnO Materials and Devices. *J. Appl. Phys.* **2005**, *98*, No. 041301.
(7) Tampo, H.; Shibata, H.; Matsubara, K.; Yamada, A.; Fons, P.; Niki, S.; Yamagata, M.; Kanie, H. Two-Dimensional Electron Gas in Zn Polar ZnMgO/ZnO Heterostructures Grown by Radical Source Molecular Beam Epitaxy. *Appl. Phys. Lett.* **2006**, *89*, No. 132113.
(8) Kato, H.; Miyamoto, K.; Sano, M.; Yao, T. Polarity Control of ZnO on Sapphire by Varying the MgO Buffer Layer Thickness. *Appl. Phys. Lett.* **2004**, *84*, 4562−4564.
(9) Hong, S. K.; Hanada, T.; Ko, H. J.; Chen, Y.; Yao, T.; Imai, D.; Araki, K.; Shinohara, M. Control of Polarity of ZnO Films Grown by Plasma-assisted Molecular-beam Epitaxy: Zn and O-polar ZnO Films on Ga-polar GaN Templates. *Appl. Phys. Lett.* **2000**, *77*, 3571−3573.
(10) Wang, X.; Tomita, Y.; Roh, O. H.; Ohsugi, M.; Che, S. B.; Ishitani, Y.; Yoshikawa, A. Polarity Control of ZnO Films Grown on Nitrided-Sapphire by Molecular-Beam Epitaxy. *Appl. Phys. Lett.* **2005**, *86*, No. 011921.
(11) Ruterana, P.; Potin, V.; Barbaray, B.; Nouet, G. Growth Defects in GaN Layers on Top of (0001) Sapphire: A Geometrical Analysis of the Misfit Effect. *Philos. Mag. A* **2000**, *80*, 937−954.
(12) Zhang, Y.; Lin, N.; Li, Y.; Wang, X.; Wang, H.; Kang, J.; Wilks, R.; Bär, M.; Mu, R. The Isotype ZnO/SiC Heterojunction Prepared by Molecular Beam Epitaxy-A Chemical Inert Interface with Significant Band Discontinuities. *Sci. Rep.* **2016**, *6*, No. 23106.
(13) Yan, Y.; Dalpian, G. M.; Al-Jassim, M. M.; Wei, S. H. Energetics and Electronic Structure of Stacking Faults in ZnO. *Phys. Rev. B* **2004**, *70*, No. 193206.
(14) Gerthsen, D.; Litvinov, D.; Gruber, T.; Kirchner, C.; Waag, A. Origin and Consequences of a High Stacking Fault Density in Epitaxial ZnO Layers. *Appl. Phys. Lett.* **2002**, *81*, 3972−3974.
(15) Yan, Y.; Al-Jassim, M. M. Inversion Domain Boundaries in ZnO: First-principles Total-Energy Calculations. *Phys. Rev. B* **2004**, *69*, No. 085204.
(16) Potin, V.; Ruterana, P.; Nouet, G.; Pond, R. C.; Morkoç, H. Mosaic Growth of GaN on (0001) Sapphire: a High Resolution Electron Microscopy and Crystallographic Study of Dislocations from Low Angle to High Angle Grain Boundaries. *Phys. Rev. B* **2000**, *61*, 5587−5599.
(17) Rhode, S. K.; Horton, M. K.; Kappers, M. J.; Zhang, S.; Humphreys, C. J.; Dusane, R. O.; Sahonta, S.-L.; Moram, M. A. Mg Doping Affects Dislocation Core Structures in GaN. *Phys. Rev. Lett.* **2013**, *111*, No. 025502.
(18) Hsu, J. W.; Manfra, P. M. J.; Lang, D. V.; Richter, S.; Chu, S. N. G.; Sergent, A. M.; Kleiman, R. N.; Pfeiffer, L. N.; Molnar, R. J. Inhomogeneous Spatial Distribution of Reverse Bias Leakage in GaN Schottky Diodes. *Appl. Phys. Lett.* **2001**, *78*, 1685−1687.
(19) Liu, B.; Yuan, F.; Dierre, B.; Sekiguchi, T.; Zhang, S.; Xu, Y. K.; Jiang, X. Origin of Yellow-Band Emission in Epitaxially Grown GaN Nanowire Arrays. *ACS Appl. Mater. Interfaces* **2014**, *6*, 14159−14166.
(20) Northrup, J. E. Shallow Electronic States Induced by Prismatic Stacking Faults in AlN and GaN. *Appl. Phys. Lett.* **2005**, *86*, No. 071901.
(21) Potin, V.; Nouet, G.; Ruterana, P. Evidence for Multiple Atomic Structures for the {1120} Inversion Domains Boundaries in GaN Layers. *Appl. Phys. Lett.* **1999**, *74*, 947−949.
(22) Northrup, J. E.; Neugebauer, J.; Romano, L. T. Inversion Domain and Stacking Mismatch Boundaries in GaN. *Phys. Rev. Lett.* **1996**, *77*, 103−106.
(23) Potin, V.; Nouet, G.; Ruterana, P. The {10-10} Inversion Domains in GaN Layers Grown on (0001) Sapphire:A Electron Microscopy Study of the Atomic Structure of the Boundaries. *Philos. Mag. A* **1999**, *79*, 2899−2919.
(24) Dimitrakopulos, G. P.; Komninou, P.; Kioseoglou, J.; Kehagias, T.; Sarigiannidou, E.; Georgakilas, A.; Nouet, G.; Karakostas, T. Structural Transition of Inversion Domain Boundaries Through Interactions with Stacking Faults in Epitaxial GaN. *Phys. Rev. B* **2001**, *64*, No. 245325.
(25) Ko, R. M.; Wang, S. J.; Chen, C. Y.; Wu, C. H.; Lin, Y. R.; Lo, H. M. Hydrothermal Growth of n-ZnO Films on a Patterned p-GaN Epilayer and its Application in Heterojunction Light-Emitting Diodes. *Jpn. J. Appl. Phys.* **2016**, *56*, No. 04CH03.
(26) O'Leary, S. K.; Foutz, B. E.; Shur, M. S.; Eastman, L. F. Steady-state and Transient Electron Transport Within Bulk Wurtzite Zinc Oxide. *Solid State Commun.* **2010**, *150*, 2182−2185.
(27) Hadi, W. A.; Chowdhury, S.; Shur, M. S.; O'Leary, S. K. A Detailed Characterization of the Transient Electron Transport within Zinc Oxide, Gallium Nitride, and Gallium Arsenide. *J. Appl. Phys.* **2012**, *112*, No. 123722.
(28) O'Leary, S. K.; Foutz, B. E.; Shur, M. S.; Lester, L. F. Steady-State and Transient Electron Transport Within the III−V Nitride Semiconductors, GaN, AlN, and InN: A Review. *J. Mater. Sci.: Mater. Electron.* **2006**, *17*, 87−126.
(29) Kaufmann, U.; Schlotter, P.; Obloh, H.; Köhler, K.; Maier, M. Hole Conductivity and Compensation in Epitaxial GaN:Mg Layers. *Phys. Rev. B* **2000**, *62*, 10867−10872.
(30) Alivov, Y. I.; Van Nostrand, J. E.; Look, D. C.; Chukichev, M. V.; Ataev, B. M. Observation of 430 nm Electroluminescence from ZnO/GaN Heterojunction Light-Emitting Diodes. *Appl. Phys. Lett.* **2003**, *83*, 2943−2945.
(31) Zhang, X. M.; Lu, M. Y.; Zhang, Y.; Chen, L. J.; Wang, Z. L. Fabrication of a High-Brightness Blue-Light-Emitting Diode Using a ZnO-Nanowire Array Grown on p-GaN Thin Film. *Adv. Mater.* **2009**, *21*, 2767−2770.
(32) Rogers, D. J.; Teherani, F. H.; Yasan, A.; Minder, K.; Kung, P.; Razeghi, M. Electroluminescence at 375nm from a ZnO/GaN:Mg/c-Al2O3 Heterojunction Light-Emitting Diode. *Appl. Phys. Lett.* **2006**, *88*, No. 141918.
(33) Yang, Q.; Wang, W.; Xu, S.; Wang, Z. L. Enhancing Light Emission of ZnO Microwire-Based Diodes by Piezo-phototronic Effect. *Nano Lett.* **2011**, *11*, 4012−4017.
(34) Schuster, F.; Laumer, B.; Zamani, R. R.; Magen, C.; Morante, J. R.; Arbiol, J.; Stutzmann, M. p-GaN/n-ZnO Heterojunction Nanowires: Optoelectronic Properties and the Role of Interface Polarity. *ACS Nano* **2014**, *8*, 4376−4384.
(35) Liu, B.; Yang, W. J.; Li, J.; Zhang, X. L.; Niu, P. J.; Jiang, X. Template Approach to Crystalline GaN Nanosheets. *Nano Lett.* **2017**, *17*, 3195−3201.
(36) Hong, S. K.; Hanada, T.; Ko, H. J.; Chen, Y.; Yao, T.; et al. Control of Crystal Polarity in a Wurtzite Crystal: ZnO Films Grown by Plasma-assisted Molecular-beam Epitaxy on GaN. *Phys. Rev. B* **2002**, *65*, No. 115331.
(37) Kobayashi, A.; Kawaguchi, Y.; Ohta, J.; Fujioka, H.; et al. Polarity Control of GaN Grown on ZnO (000-1) Surfaces. *Appl. Phys. Lett.* **2006**, *88*, No. 181907.
(38) Ullah, M. B.; Avrutin, V.; Li, S. Q.; Das, S.; Monavarian, M.; Toporkov, M.; Özgür, Ü.; Ruterana, P.; Morkoç, H. Polarity Control and Residual Strain in ZnO Epilayers Grown by Molecular Beam Epitaxy on (0001)-GaN/Sapphire. *Phys. Status Solidi RRL* **2016**, *10*, 682−686.
(39) Austerman, S. B.; Gehman, W. G. The Inversion Twin: Prototype in Beryllium Oxide. *J. Mater. Sci.* **1966**, *1*, 249−260.
(40) Kim, J. C.; Goo, E. Inversion Domain Boundaries in Zinc Oxide. *J. Am. Ceram. Soc.* **1990**, *73*, 877−884.
(41) De la Mata, M.; Magen, C.; Gazquez, J.; Iqbal Bakti Utama, M.; Heiss, M.; Lopatin, S.; Furtmayr, F.; Fernandez-Rojas, C. J.; Peng, B.; Morante, J. R.; Rurali, R.; Eickhoff, M.; Morral, A. F.; Xiong, Q.; Arbiol, J. Polarity Assignment in ZnTe, GaAs, ZnO, and GaN-AlN Nanowires from Direct Dumbbell Analysis. *Nano Lett.* **2012**, *12*, 2579−2586.

DOI: 10.1021/acsami.8b12202
ACS Appl. Mater. Interfaces 2018, 10, 37651−37660

(42) Kresse, G.; Joubert, J. Efficient Iterative Schemes for ab initio Total-energy Calculations Using a Plane-wave Basis Set. *Phys. Rev. B* **1996**, *54*, 11169−11186.
(43) Hafner, J. Ab-Initio Simulations of Materials Using VASP: Density-Functional Theory and Beyond. *J. Comput. Chem.* **2008**, *29*, 2044−2078.
(44) Kresse, G.; Joubert, J. From Ultrasoft Pseudopotentials to the Projector Augmented-Wave Method. *Phys. Rev. B* **1999**, *59*, 1758−1775.
(45) Li, S. Q.; Lei, H. P.; Wang, Z.; Chen, J.; Ruterana, P. Energetic and Electronic Properties of (0001) Inversion Domain Boundaries in ZnO. *Phys. Status Solidi B* **2018**, *255*, No. 1700429.
(46) Becke, A. D.; Edgecombe, K. E. A Simple Measure of Electron Localization in Atomic and Molecular Systems. *J. Chem. Phys.* **1990**, *92*, 5397−5403.
(47) Savin, A.; Jepsen, O.; Flad, J.; Andersen, O. K.; Preuss, H.; Von Schnering, H. G. Electron Localization in Solid-state Structures of the Elements: the Diamond Structure. *Angew. Chem., Int. Ed.* **1992**, *31*, 187−188.
(48) Silvi, B.; Savin, A. Classification of Chemical Bonds Based on Topological Analysis of Electron Localization Functions. *Nature* **1994**, *371*, 683−686.
(49) Kowalczyk, S. P.; Ley, L.; Pollak, R. A.; McFeely, F. R.; Shirley, D. A. Relative Effect of Extra-atomic Relaxation on Auger and Binding-energy Shifts in Transition Metals and Salts. *Phys. Rev. B* **1974**, *9*, 381−391.
(50) Wei, S.-H.; Zunger, A. Role of Metal d states in II-VI Semiconductors. *Phys. Rev. B* **1988**, *37*, 8958−8981.
(51) Janotti, A.; Segev, D.; Van de Walle, C. G. Effects of Cation d States on the Structural and Electronic Properties of III-nitride and II-oxide Wide-band-gap Semiconductors. *Phys. Rev. B* **2006**, *74*, No. 045202.

DOI: 10.1021/acsami.8b12202
ACS Appl. Mater. Interfaces 2018, 10, 37651−37660